How hybrid excitons suppress charge separation: ultrafast, but delayed

Lukas Gierster[1,2*], Olga Turkina[3], Jan-Christoph Deinert[1], Sesha Vempati[1], Elsie Bowen Dodoo[1], Yves Garmshausen[2], Stefan Hecht[2], Claudia Draxl[3] and Julia Stähler[1,2*]

[1]Department of Physical Chemistry, Fritz-Haber-Institut der Max-Planck-Gesellschaft, Faradayweg 4-6, Berlin, 14195, Germany.
[2]Institut für Chemie, Humboldt-Universität zu Berlin, Brook-Taylor-Str. 2, Berlin, 12489, Germany.
[3]Institut für Physik und IRIS Adlershof, Humboldt-Universität zu Berlin, Newtonstr. 15, Berlin, 12489, Germany.

*Corresponding author(s). E-mail(s): lukas.gierster@hu-berlin.de; julia.staehler@hu-berlin.de;
Contributing authors: turkina@physik.hu-berlin.de;

Abstract

Inorganic/organic hybrid systems offer great technological potential for novel solar cell design due to the combination of high charge carrier mobilities in the inorganic semiconductor with the chemical tuneability of organic chromophore absorption properties. While ZnO basically exhibits all necessary properties for a successful application in light-harvesting, it was clearly outpaced by TiO_2 in terms of charge separation efficiency. The physical origin of this deficiency is still under debate. Here, we use a combination of femtosecond time-resolved photoelectron spectroscopy with many-body *ab initio* calculations to demonstrate that optical excitation of the chromophore is followed by (1) ultrafast electron transfer into the ZnO bulk (350 fs), (2) electron relaxation, and (3) delayed (100 ps) recapture of the electrons at a 1 nm distance from the interface in (4) a strongly bound (0.7 eV) hybrid exciton state with a lifetime exceeding 5 μs that is analysed by taking into account pump-probe delay-dependent photostationary population

dynamics. Beyond this identification and quantification of all elementary steps leading to the suppression of charge separation at ZnO interfaces, our key finding is the substantially delayed hybrid exciton formation. It opens up a sufficiently large time window for counter-measures with the potential to finally successfully implement ZnO in light-harvesting or optoelectronic devices without significant efficiency losses.

Keywords: hybrid system, excitons, charge transfer, ultrafast

Driven by the rising demand for renewable energies, tremendous efforts are made to find cost-effective alternatives for silicon solar cells [1]. Hybrid systems consisting of molecules with strong absorbance of sun light and semiconductors with high charge carrier mobilities promise to be a solution, for example Grätzel-type solar cells [2]. TiO_2 is the most commonly used semiconductor, but ZnO is a very widely investigated alternative [2, 3] and actually even expected to perform better due to its higher electron mobility and ease of nanostructure fabrication [3]. However, the charge conversion efficiencies of ZnO-based systems are still lower than those using TiO_2. Nevertheless, considerable progress was achieved recently by doping and core-shell structures combining ZnO with TiO_2 [2].

Despite extensive efforts, the origin of the lower charge conversion efficiency of ZnO is still under debate [4]. While, depending on the chromophore, the photoinjection of electrons into TiO_2 can occur in the sub-ps time domain [2], the injection into ZnO is reported to be delayed and to occur in a two-step process of several hundreds of femtoseconds and few to hundreds of picoseconds [5]. This allows for electron-hole recombination before charge separation occurs, leading to losses in the solar cell performance [6]. For decades, several options are discussed to explain this difference: (i) the lower density of conduction band states in ZnO compared to TiO_2 [7], (ii) long-lived molecular [8] or interfacial trap states [5], which both depend on the molecules used, and (iii) hybrid charge transfer excitons or hybrid excitons (HX) for short, i.e. interfacial electron-hole pairs with the electron in the inorganic and the hole in the organic layer, which trap the charges at the interface. In the latter case, the binding forces should be much stronger for ZnO due to the lower dielectric constant compared to TiO_2 ($\epsilon_{\mathrm{ZnO}} = 8$, $\epsilon_{\mathrm{TiO_2}} = 80$ [2]). Many authors favour this scenario to explain the ultrashort dynamics on fs to few ps time scales [4, 9–12]. However, systematic variation of molecule length and, thus, the position of the photohole with respect to the interface, shows no dominant effect on the ultrafast dynamics [5].

HX at ZnO/organic interfaces were indirectly observed in electroluminescence studies that show light emission matching the energy difference of the ZnO CB and the HOMO of the molecule minus a reorganization energy of several hundred meV [13–15]. They are also reported to affect solar cell performance [16], as do charge-transfer excitons in all-organic solar cells [17]. Clearly,

direct experimental access to the formation dynamics of hybrid excitons at ZnO interfaces is needed to confirm their impact on the charge separation efficiencies and develop strategies to circumvent their detrimental influence.

A *direct* measurement of hybrid excitons and their formation dynamics is, unfortunately, still missing. The widely used transient absorption spectroscopy is not sensitive to electron localisation and relies on optical transition dipole moments. Beyond optical approaches, however, progress has been made recently: changes to the potential energy surfaces on timescales between 10's of ps up to μs were attributed to the formation of localised electrons in ZnO within <6 nm to the interface using time-resolved X-ray photoelectron spectroscopy [4]. These results are in line with the observation of defect excitons at ZnO surfaces [18] and ultrafast THz spectroscopy, which detects electrons retained at the interface for times exceeding the ps range after ultrafast photoinjection [9]. Although these works are indicative of long-lived hybrid excitons, an unambiguous assignment, including knowledge of the formation pathway, (lateral) localisation, and binding energy of the trapped electrons is still lacking. Knowledge of the elementary steps of photoinjection as well as hybrid exciton formation is indispensable in order to not only decide if efficient charge separation is at all possible at ZnO interfaces, but imperative to develop strategies against interfacial trapping in general.

We disentangle the charge injection and hybrid exciton formation at a ZnO/organic interface using time-resolved two-photon photoelectron spectroscopy (TR-2PPE) combined with *ab initio* many-body perturbation theory, employing the Bethe Salpeter equation (BSE). To enable comparison between experiment and theory, we use a well-characterized [19] model system consisting of a single crystal ZnO surface and a tailored organic molecule, *p*-quinquephenyl-pyridine (5P-Py, see inset in Fig. 1d). We isolate the impact of electronic coupling and electron-hole Coulomb interaction and observe sub-ps charge injection dynamics by following the non-equilibrium population dynamics of the lowest unoccupied molecular orbital (LUMO) using two distinct excitation pathways, *interfacial* and *intramolecular*, as illustrated in Fig. 1b,c. Based on this, we can rule out that (i) density of state effects and (ii) molecular or interfacial trap states hinder electron injection. On the contrary, after the electrons transfer to ZnO on femtosecond timescales, they escape from the probed volume into the bulk of the semiconductor. Remarkably, however, the electrons *return* to the interface within 100(50) ps. They populate an electronic state at 0.71(5)-0.91(5) eV below the conduction band (CB) minimum, in good agreement with our BSE calculations that yield a binding energy of 0.7 eV for hybrid excitons localised at a 1 nm distance from the photohole. The HX lifetime exceeds the inverse laser repetition rate of 5 μs, leading to a photostationary state in our experiments. This study reveals the complete charge transfer sequence at a model inorganic-organic interface and resolves the long-standing issue of low ZnO performance in hybrid solar cells. Not only is ultrafast electron injection into ZnO clearly possible at rates comparable to record values reported for TiO_2 [20]; we find that HX formation proceeds by

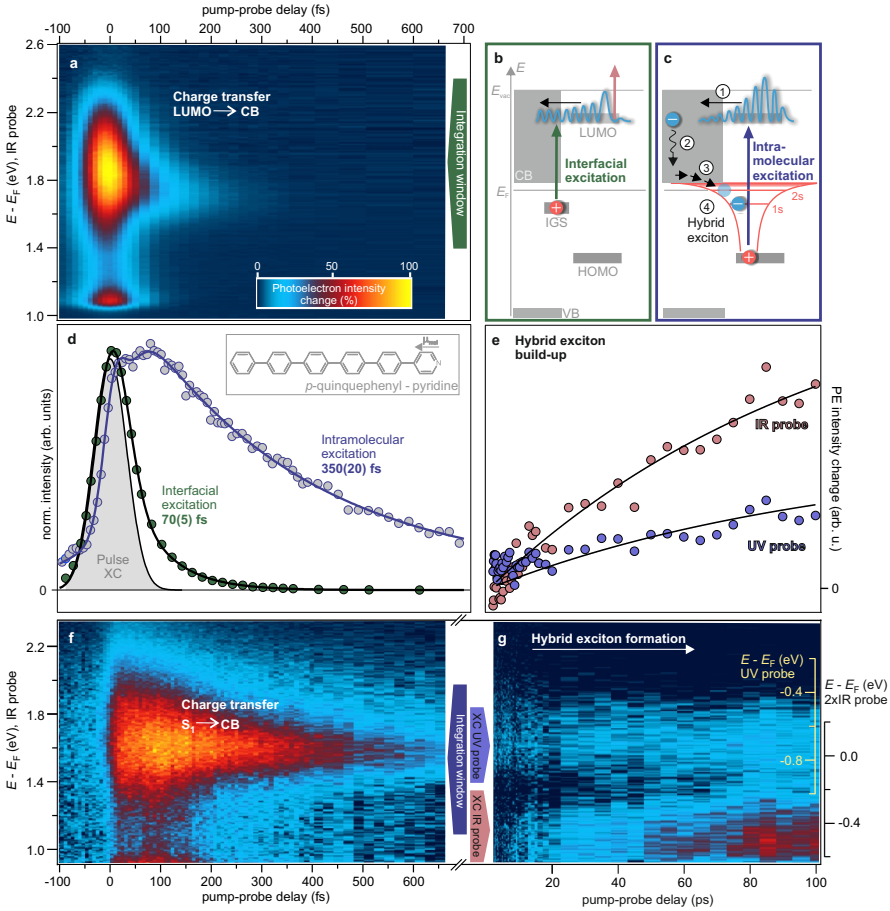

Fig. 1 Ultrafast electron transfer dynamics followed by HX formation. a, Time-resolved PE intensity change (false colours) of LUMO population after interfacial excitation with $h\nu_{\mathrm{pump}} = 2.52$ eV, $h\nu_{\mathrm{probe}} = 1.53$ eV. **b,c,** Schematics of interfacial and intramolecular excitation. **d,** Time-dependent PE signal for interfacial (green) and intramolecular excitation (blue) and laser pulses' envelope (grey). Inset: 5P-Py molecule. **e,** Hybrid exciton population build-up extracted from Fig. 1g including fit of the pump-probe delay-dependent changes to photostationary state intensities. **f,** Time-resolved PE intensity change (false colours) of the S_1 population after intramolecular excitation with $h\nu_{\mathrm{pump}} = 3.9$ eV, $h\nu_{\mathrm{probe}} = 1.55$ eV. **g,** Build-up of hybrid exciton population probed via changes to the photostationary state intensity of UV (yellow energy axis) and IR photons (black energy axis, right).

delayed attraction of electrons to the interface. These observations suggests that efficient hybrid solar cells can be designed using ZnO if interfacial trapping is avoided by funneling either photoholes or -electrons away from the interface within the hybrid exciton formation time of 100(50) ps.

Figure 1a shows the time-dependent photoelectron intensity change as a function of energy with respect to E_{F} and pump-probe time delay Δt after

interfacial excitation ($h\nu_{\text{pump}} = 2.52$ eV) as illustrated in Fig. 1b. As outlined in a previous study of the same system [19], electrons are promoted from an occupied in-gap state (IGS) to the 5P-Py LUMO. At temporal overlap ($\Delta t = 0$) of pump and probe ($h\nu_{\text{probe}} = 1.53$ eV), an intense signal is observed. It peaks at 1.86 eV and has a full width at half maximum of 0.5 eV in agreement with previous work [19]. This non-equilibrium population of the LUMO fully decays within few hundred fs. The band integral across the peak yields the green cross correlation (XC) trace in Fig. 1d, which can be accurately fitted with a single exponential decay with $\tau_{\text{interface}} = 70(5)$ fs convolved with the laser pulses' envelope (grey in Fig. 1d, see Methods for details). This population decay of the LUMO is much faster than typical electron-hole recombination times in organic molecules [21, 22] and attributed to charge transfer into the ZnO CB. We conclude that the LUMO is strongly coupled to the CB and that low charge separation efficiencies cannot result from a low density of states in ZnO, as efficient charge transfer is evidently possible.

We address the impact of a photohole on the charge transfer dynamics by resonantly exciting the 5P-Py molecules at their absorption maximum [19]. With this *intramolecular excitation*, the electron wave function is expected to be more localised on the molecule (cf. schematic in Fig. 1c) thereby reducing wave function overlap with the ZnO and, consequently, reducing the transfer rate. In order to avoid bulk effects of the organic film, we ensure monolayer coverage (Methods). Fig. 1f shows the excited state population dynamics after *intramolecular* excitation, lasting up to 1 ps, i.e. considerably longer than upon *interfacial* excitation. For quantitative comparison, the spectrally integrated intensity evolution is shown in Fig. 1d. Again, a single exponential population decay fits the data (see Methods for more details). The time constant $\tau_{\text{molecule}} = 350(20)$ fs is five times larger than $\tau_{\text{interface}}$ and, thus, the photoinjection is slower due to the attractive Coulomb interaction of the hole in the molecular film, as expected. Nevertheless, the time constant is still ultrafast and, hence, the coupling is strong. We conclude that the influence of the hole on the ultrafast photoinjection is minor, in agreement with Ref. [5], and that the reduced charge conversion efficiencies at ZnO interfaces must have a different origin.

To elucidate the cause for suppressed charge separation, we perform *ab initio* calculations of nP-Py/ZnO ($n = 0, 1, 2$ phenyl rings attached to pyridine) interfaces. Our calculations show that the HOMOs are quite localised on nP-Py as illustrated by the charge density plots in Fig. 2a. They do, however, weakly extend into the ZnO. BSE calculations (see Supplementary Material (SM) and Ref. [23] for details) show that a hybrid exciton can be formed with a binding energy of 0.2 eV. Figure 2b shows the quasiparticle band structure of Py/ZnO (the corresponding results for $n = 1, 2$ can be found in the SM) and illustrates by the colour code the respective contribution of the electron (light blue) and hole (light red) to the HX wave function. Note that the hole is in the HOMO of the molecule.

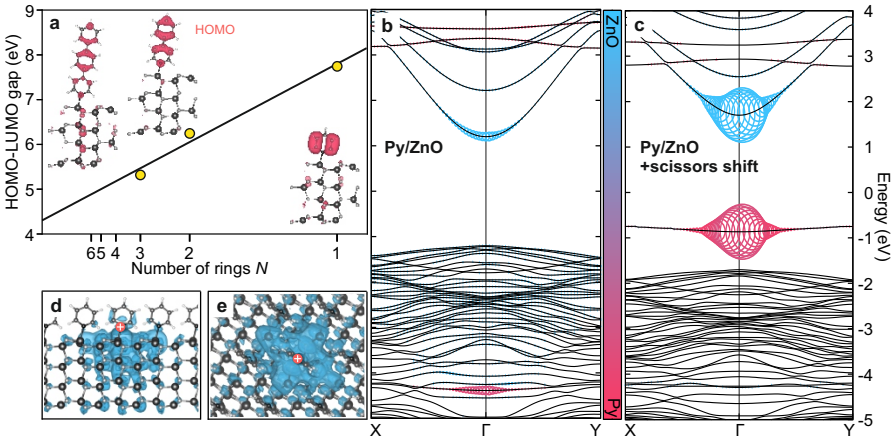

Fig. 2 Electronic structure and hybrid excitons at nP-Py interfaces. a, HOMO-LUMO gap and HOMO electron density of nP-Py as calculated by DFT with the number of rings including the pyridine unit $N = n + 1$. **b,** Band structure of Py/ZnO(10-10) as calculated by DFT+GW and hybrid exciton contributions based on BSE. **c,** Analogous calculations for the HOMO scissor-shifted into the band gap as observed in the experiment and adjusted ZnO band gap. **d,e** Side and top view of the electron distribution of the exciton wave function, with the hole localised at the molecule (red dots).

Unfortunately, a full many-body treatment consisting of the GW approximation and a subsequent BSE calculation for the experimentally investigated 5P-Py molecule is computationally not feasible. We therefore use a simplified approach to simulate the HX at the 5P-Py/ZnO interface. Thereby, we make use of the fact that the band gap of nP-Py shrinks linearly with the inverse number of rings (cf. Fig. 2a) as commonly known for such conjugated systems. Experimentally, we determined the position of the LUMO 1.8 eV above the Fermi energy, i.e. 1.6 eV above the ZnO CB minimum, and the optical gap to be 3.9 eV [19]. ZnO exhibits a wide band gap of 3.4 eV [24]. Accordingly, we adjust the HOMO-LUMO distance and the ZnO band gap by scissors shifts applied to the DFT bands of Py/ZnO. The resulting band structure is displayed in Fig. 2c. This "trick" is justified as the character of the bands involved in the HX are the same in all the systems. The BSE calculation based on these bands yields the HX with an increased binding energy of 0.7 eV due to the stronger localisation of the photohole on the molecule, since the HOMO is now residing in the ZnO band gap. Figures 2d and e show the electron density distribution (40 % equal density surface) of the HX wave function with the hole position fixed on the molecule. Clearly, the electron is residing in the ZnO. Integration of the charge density (cf. SM) shows that 78 % of the electron density resides in the first nm of the ZnO with a lateral full width at half maximum of 1.4 nm.

Note that the large HX binding energy suggests that the electronic level of the hybrid exciton, which would be probed in photoemission, lies significantly below the conduction band minimum of ZnO (cf. Fig. 1c), which is located at only 0.2 eV above the Fermi energy E_F [25]. This would quench all potential

HX decay channels except for recombination, as all available electronic states (even within several 100 meV) are occupied below E_F. This would inevitably lead to long lifetimes in the order of 100's of ps [26, 27], ns [28], or even up to μs [18], possibly exceeding the inverse repetition rate of our laser system (5 μs), such that a photostationary population could be detected even in single-colour photoemission experiments [18] (details will be discussed below). In order to probe such metastable states at low energies, either (UV) photon energies exceeding the work function $\Phi = E_{vac} - E_F$ are needed, or multiphoton photoemission with IR or VIS photons is required as illustrated in the inset of Fig. 3a.

The blue spectrum in Fig. 3a shows the single-colour ($h\nu_{UV} = 3.90$ eV) 1PPE intensity distribution as a function of final state energy. Beyond the secondary electron tail that is cut off at 2.4 eV, indicating the low work function of the 5P-Py sample, the spectrum exhibits a broad peak at $E_{final} - E_F = 3.19(5)$ eV, corresponding to an initial state energy of 0.71(5) eV below E_F (cf. grey energy axis). The same signature is also detected in the red single-colour ($h\nu_{IR} = 1.55$ eV) 2PPE spectrum in Fig. 3a. It is located at lower final state energy due to the photon energy difference $\Delta h\nu = h\nu_{UV} - 2h\nu_{IR}$ and, therefore, superimposed with the secondary electron tail. With respect to the bulk conduction band minimum of our ZnO sample, which lies 0.2 eV above E_F [24], the state has, no matter whether it is probed by UV or IR light, a binding energy of 0.91(5) eV. However, downward surface band bending at the surface of ZnO(10-10) up to E_F was observed before [18, 24] and is highly likely also for the interface with 5P-Py, not least because of the strongly reduced work function. Based on this, we deduce an experimental binding energy of 0.71(5)-0.91(5) eV, which is in excellent agreement with our calculations.

To test the hypothesis that the state observed in the single-colour spectra is resulting from a photostationary HX population, we inspect the nature of this state by comparison of the sum of the single colour spectra (grey line) with two-colour PE spectra at negative pump-probe time delays (black line). If the electronic state were originating from an ordinary occupied state, no correlation of the laser pulses should be observed and the negative delay spectrum should coincide with the sum of the single-colour spectra. Clearly, this is not the case: Both, the UV- and IR-probed peaks, have larger intensities in the black spectrum, when both colours are used in the experiment, demonstrating a *correlation* between laser pulses.

This observation can be understood when considering an excited state lifetime exceeding the inverse repetition rate of the laser system ($1/R = 5$ μs). In single-colour PE, each consecutive laser pulse populates and depopulates the long-lived species, leading to the build-up of a photostationary state with an intensity that depends on the (de)population probabilities as illustrated by Fig. 3c,d. When both colours are used, separated e.g. by a pump-probe delay $\Delta t > 0$ (cf. Fig. 3b), the excited state population generated by the UV may be probed by IR photons and vice versa. A *correlated* photostationary state

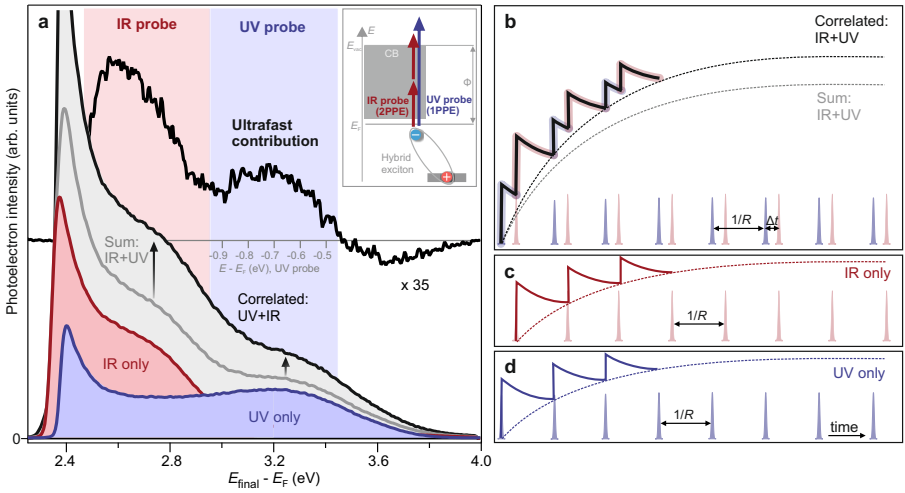

Fig. 3 Long-lived hybrid excitons as photostationary states in PE spectra. a, Comparison of single colour PE spectra (blue, red) and their sum (grey) with correlated signals (black). Difference spectrum for $\Delta t = +85$ ps and -3 ps is offset and upscaled for clarity. Inset: The hybrid exciton is probed by IR and UV photons in a 2PPE and 1PPE process, respectively. **b-d,** Build-up of photostationary states for (d) UV and (c) IR illumination only, as well as for two-colour experiments.

(PSS) is detected (black) that has a different intensity than the mere sum of the single-colour signals (grey).

It is tempting to assume that a photo*stationary* state does not exhibit any dynamics once it is built-up. However, a PSS is only stationary with respect to the fixed pump-probe delay Δt at which the spectrum is taken. In other words, for different Δt, different PSS may form, for instance because the succeeding pulse interferes with the formation dynamics of the transient species launched by the preceding laser pulse as outlined in detail in the SM and in Ref. [29]. Subtraction of photostationary spectra at different Δt yields such dependence of the PSS intensity on the pump-probe time delay.

The black, unfilled spectrum in Fig. 3a is a representative difference spectrum generated by subtracting $\Delta t = -3$ ps data from the spectrum at +85 ps. It is shifted upwards for clarity and significantly upscaled (x35). The spectrum illustrates that the average PSS population is only slightly, but notably higher if the UV photons are absorbed 85 ps *before* the IR pulse arrives than if the UV pulse succeeds the VIS pulse by 3 ps. In other words, the photostationary population is higher for a pulse train with $\Delta t = 85$ ps. Based on this, we conclude that intramolecular excitation of 5P-Py leads, in addition to the ultrafast electron transfer discussed above, to the build-up of a photostationary state with a high binding energy of 0.71(5)-0.91(5) eV with respect to the ZnO CB continuum that exhibits lifetimes larger than 5 μs. This experimental observation confirms the theoretical prediction described above that anticipates a hybrid exciton with a binding energy of 0.7 eV. It results in very long excited state lifetimes due to the strong n-doping of ZnO.

Having demonstrated that the PSS differs for different pump-probe time delays Δt, we return to the time-resolved data after intramolecular excitation in Fig. 1. Panel g shows the time-dependent change of the PE intensity for pump-probe delays up to 100 ps. Note that the complete 5P-Py S_1 population has decayed after the first few ps by charge transfer to the ZnO as discussed above, and the PE intensity is in the noise floor. After ca. 10 ps, a slow intensity build-up is observed, at the initial state energy of the photostationary hybrid exciton state. As discussed above, it appears in a double peak structure due to probing by photoemission with IR *and* UV photons (yellow and black axes on the right), respectively, which is possible due to the long lifetime of this species. Band integrals of both peaks result in the transients in Fig. 1e. A global single exponential fit (black lines) yields a rise time of 100(50) ps.

Based on the above findings, we are able to describe the complete sequence of elementary steps that lead to hybrid exciton formation at organic-ZnO interfaces, also illustrated in Fig. 1b and c: Photoexcitation of the chromophore is followed by (1) ultrafast electron transfer to the ZnO, competing with record charge injection times of TiO_2 [20]. This electron transfer is only marginally slowed down by the presence of the photohole on the molecule. The relaxation (2) of the injected electrons is not detected by photoemission, which means that the carriers have left the surface region. It is, however, known [26, 30] that electrons reach the minimum of the conduction band quickly on sub-picosecond timescales. Remarkably, after a substantial delay, the electrons are (3) recaptured at the interface. The hybrid exciton signal builds up with a time constant of 100(50) ps. This can be rationalized by the long-range Coulomb attraction of the photohole on the chromophore, which is less screened in ZnO than in TiO_2. Due to the very large binding energy of the hybrid exciton (4), it takes time for the exciton to reach the 1s state within the Rydberg-like series of of electron states within the potential of the hole, as several 100 meV need to be released upon cooling of the hot exciton (cf. Fig. 1c). Moreover, the majority of the HX decay channels is blocked, as all electronic levels are filled up to the Fermi energy. The 1s hybrid exciton can solely decay by recombination. This leads to very long lifetimes beyond 5 μs.

This new and detailed understanding of the delayed formation of hybrid excitons is not only consistent with previous findings in the literature as, for instance, the high binding energy from electroluminescence studies [13, 14] or the long lifetime of interfacial trapped electrons in time-resolved XPS [4]. It also directs us towards concerted strategies to circumvent the hybrid exciton formation for enhanced charge separation. Knowing that electrons are *re*captured at the interface due to the attractive Coulomb potential of the photohole, it is now clear why doping or core shell structures enhancing the screening of the Coulomb interaction successfully enhanced the charge separation efficiency in the past [2] and could possibly be further optimized.

The prime insight of this work is, however, the finding that hybrid exciton formation occurs in a *delayed* fashion, with a quite substantial build-up time

of 100 ps. This comfortable time window opens up possibilities to funnel photocarriers away from the interface *before* they bind in the form of stable 1s hybrid excitons. Electron capture at the backside of sufficiently thin ZnO films is equally conceivable as scavenging photoholes in the chromophores by using appropriate hole acceptors, or manipulation of the potential energy landscape by built-in electric fields.

1 Methods

1.1 Sample preparation

Sample preparation is performed in a UHV chamber with a base pressure below $5 \cdot 10^{-10}$ mbar. Single crystal ZnO(10-10) samples (MaTecK GmbH) are prepared by Ar^+ sputtering (0.75 keV, 10 min) and annealing cycles at 700-900 K for 30 min following established procedures [31]. The surface reconstruction is confirmed with LEED. The 5PPY molecule is a derivative of the widely used sexiphenyl, with a Nitrogen atom at the end to bind in an ordered fashion at the ZnO surface, for details on the synthesis see ref. [19]. 5PPy molecules are evaporated (0.3-0.7 nm/min) from a Knudsen cell onto the freshly prepared ZnO(10-10) surface after carefully degassing of the molecules at 10 K below their evaporation temperature of ca. 530 K. A pre-calibrated quartz crystal microbalance is employed to estimate the thickness of the film. The adsorption of 5PPy on ZnO(10-10) also induces a work function change that is characteristic of the film thickness; a minimum work function of 2.45(5) eV is reached at 1 ML [19], corresponding to the data shown in Fig. 1 f (intramolecular excitation).

1.2 Photoelectron spectroscopy

After preparation, the sample is transferred *in situ* to the analyzer chamber. Photoelectrons are detected using a hemispherical analyzer (Phoibos 100, SPECS) with an energy resolution of ca. 50 meV. During the photoemission experiments the sample temperature is held at 100 K, and the pressure is kept $<10^{-10}$ mbar. A bias voltage V_{bias} of -2.5 to -5.5 V is applied to the sample with respect to the analyzer enabling the detection of electrons with zero kinetic energy, which constitute the secondary electron cutoff. The spectra are referenced to the Fermi level E_{F} measured at the gold sample holder, which is in electrical contact with the sample. Note that the kinetic energy of E_{F} scales with the photon energy $\mathrm{h}\nu$, as the measured kinetic energy of electrons originating from E_{F} is $E_{\mathrm{kin}}(E_{\mathrm{F}}) = \mathrm{h}\nu - \Phi_{\mathrm{Analyzer}} - eV_{\mathrm{bias}}$, where Φ_{Analyzer} is the work function of the electron analyzer. The pump and probe laser pulses are generated by a femtosecond 200 kHz laser system (Light Conversion), consisting of a regenerative amplifier (Pharos) feeding two non-collinear optical paramteric amplifiers (Orpheus 2H/3H). Pulse durations are on the order of 30-50 fs. For the intramolecular excitation the pump laser fluence is kept low

(0.2 μJ/cm^2) due to strong direct photoemission (the pump photon energy of 3.9 eV is larger than the sample work function). The probe laser fluence is 700 μJ/cm^2. Due to the high power, 2PPE with the probe laser beam from occupied states is about as efficient as direct photoemission with the pump laser beam.

1.3 Data representation and fitting

In the TR-2PPE spectra presented in Fig. 1 a,f,g the photoemission background at negative delay times (-2 ps) was subtracted to show the excited state dynamics. The fitting of the photoelectron intensity transients in Fig. 1 d is done for interfacial excitation with

$$f(\Delta t) = Ae^{-\Delta t^2} + Be^{-\Delta t/\tau_{\mathrm{decay}}}$$

and for intramolecular excitation with

$$f(\Delta t) = Ae^{-\Delta t^2} + Be^{-\Delta t/\tau_{\mathrm{decay}}}(1 - e^{-\Delta t/\tau_{\mathrm{rise}}}).$$

The first term in both fit functions is a narrow Gaussian function (width 1 fs) to account for two-colour 2PPE via virtual states without populating the LUMO from the IGS/the HOMO. A delayed rise ($\tau_{\mathrm{rise}} = 80(10)$ fs) of the LUMO population is observed upon intramolecular excitation, which is likely attributed to internal conversion; two colour 2PPE and delayed rise leads to the double peak structure in the data (cf. Fig. 1 d). The functions are convoluted with the laser pulses' cross-correlation measured at the gold sample holder before fitting them to the data.

1.4 Theory

All calculations have been carried out with the all-electron full-potential code `exciting` [32], based on the frameworks of density-functional theory and many-body perturbation theory. Details are provided in the SM. All input and output files of the calculations can be downloaded from NOMAD [33] under the DOI 10.17172/NOMAD/2023.06.14-1

Supplementary information. Details on the calculations, details on femtosecond dynamics of photostationary states.

Acknowledgments. We acknowledge funding by the Deutsche Forschungsgemeinschaft (DFG, German Research Foundation) - Project-ID 182087777 - SFB 951.

Author contributions. LG and SV performed the main experiments. JCD took preliminary experiments, LG and EBD performed reproducibility tests. YG and SH synthesized the 5P-Py molecules. OT performed all calculations. The initial idea of the project was developed by SH, CD and JS. Data analysis was done by LG in close exchange with JS. LG, OT, CD, and JS led the discussion of the results by all co-authors. OT and CD wrote the theoretical and LG and JS wrote the experimental and general parts of the manuscript.

Competing interests. The authors declare no competing interests.

Editorial Policies for:

Springer journals and proceedings:
https://www.springer.com/gp/editorial-policies

References

[1] Polman, A., Knight, M., Garnett, E.C., Ehrler, B., Sinke, W.C.: Photovoltaic materials: Present efficiencies and future challenges. Science **352**(6283) (2016). https://doi.org/10.1126/science.aad4424

[2] Muñoz-García, A.B., Benesperi, I., Boschloo, G., Concepcion, J.J., Delcamp, J.H., Gibson, E.A., Meyer, G.J., Pavone, M., Pettersson, H., Hagfeldt, A., Freitag, M.: Dye-sensitized solar cells strike back. Royal Society of Chemistry (2021). https://doi.org/10.1039/d0cs01336f

[3] Wibowo, A., Marsudi, M.A., Amal, M.I., Ananda, M.B., Stephanie, R., Ardy, H., Diguna, L.J.: ZnO nanostructured materials for emerging solar cell applications. RSC Advances **10**(70), 42838–42859 (2020). https://doi.org/10.1039/D0RA07689A

[4] Neppl, S., Mahl, J., Roth, F., Mercurio, G., Zeng, G., Toma, F.M., Huse, N., Feulner, P., Gessner, O.: Nanoscale Con fi nement of Photo-Injected Electrons at Hybrid Interfaces (2021). https://doi.org/10.1021/acs.jpclett.1c02648

[5] Strothkämper, C., Bartelt, A., Sippel, P., Hannappel, T., Schütz, R., Eichberger, R.: Delayed electron transfer through interface states in hybrid ZnO/organic-dye nanostructures. Journal of Physical Chemistry C **117**(35), 17901–17908 (2013). https://doi.org/10.1021/jp402042a

[6] Sobuś, J., Burdziński, G., Karolczak, J., Idígoras, J., Anta, J.A., Ziółek, M.: Comparison of TiO2and ZnO solar cells sensitized with an indoline dye: Time-resolved laser spectroscopy studies of partial charge separation processes. Langmuir **30**(9), 2505–2512 (2014). https://doi.org/10.1021/la404782s

[7] Wei, H., Luo, J.W., Li, S.S., Wang, L.W.: Revealing the Origin of Fast Electron Transfer in TiO2-Based Dye-Sensitized Solar Cells. Journal of the American Chemical Society **138**(26), 8165–8174 (2016). https://doi.org/10.1021/jacs.6b03524

[8] Borgwardt, M., Wilke, M., Kampen, T., Mähl, S., Xiao, M., Spiccia, L., Lange, K.M., Kiyan, I.Y., Aziz, E.F.: Charge Transfer Dynamics at

Dye-Sensitized ZnO and TiO2 Interfaces Studied by Ultrafast XUV Photoelectron Spectroscopy. Scientific Reports **6**, 1–7 (2016). https://doi.org/10.1038/srep24422

[9] Němec, H., Rochford, J., Taratula, O., Galoppini, E., Kužel, P., Polívka, T., Yartsev, A., Sundström, V.: Influence of the electron-cation interaction on electron mobility in dye-sensitized ZnO and TiO2 nanocrystals: A study using ultrafast terahertz spectroscopy. Physical Review Letters **104**(19), 1–4 (2010). https://doi.org/10.1103/PhysRevLett.104.197401

[10] Vaynzof, Y., Bakulin, A.A., Gélinas, S., Friend, R.H.: Direct observation of photoinduced bound charge-pair states at an organic-inorganic semiconductor interface. Physical Review Letters **108**(24), 1–5 (2012). https://doi.org/10.1103/PhysRevLett.108.246605

[11] Siefermann, K.R., Pemmaraju, C.D., Neppl, S., Shavorskiy, A., Cordones, A.A., Vura-Weis, J., Slaughter, D.S., Sturm, F.P., Weise, F., Bluhm, H., Strader, M.L., Cho, H., Lin, M.F., Bacellar, C., Khurmi, C., Guo, J., Coslovich, G., Robinson, J.S., Kaindl, R.A., Schoenlein, R.W., Belkacem, A., Neumark, D.M., Leone, S.R., Nordlund, D., Ogasawara, H., Krupin, O., Turner, J.J., Schlotter, W.F., Holmes, M.R., Messerschmidt, M., Minitti, M.P., Gul, S., Zhang, J.Z., Huse, N., Prendergast, D., Gessner, O.: Atomic-scale perspective of ultrafast charge transfer at a dye-semiconductor interface. Journal of Physical Chemistry Letters **5**(15), 2753–2759 (2014). https://doi.org/10.1021/jz501264x

[12] Furube, A., Katoh, R., Hara, K.: Electron injection dynamics in dye-sensitized semiconductor nanocrystalline films. Surface Science Reports **69**(4), 389–441 (2014). https://doi.org/10.1016/j.surfrep.2014.09.003

[13] Piersimoni, F., Schlesinger, R., Benduhn, J., Spoltore, D., Reiter, S., Lange, I., Koch, N., Vandewal, K., Neher, D.: Charge transfer absorption and emission at ZnO/organic interfaces. Journal of Physical Chemistry Letters **6**(3), 500–504 (2015). https://doi.org/10.1021/jz502657z

[14] Panda, A., Ding, K., Liu, X., Forrest, S.R.: Free and trapped hybrid charge transfer excitons at a ZnO/small-molecule heterojunction. Physical Review B **94**(12), 1–7 (2016). https://doi.org/10.1103/PhysRevB.94.125429

[15] Hörmann, U., Zeiske, S., Piersimoni, F., Hoffmann, L., Schlesinger, R., Koch, N., Riedl, T., Andrienko, D., Neher, D.: Stark Effect of Hybrid Charge Transfer States at Planar ZnO/Organic Interfaces **155312**, 9–13 (2018). https://doi.org/10.1103/PhysRevB.98.155312

[16] Eyer, M., Frisch, J., Sadofev, S., Koch, N., List-Kratochvil, E.J.W., Blumstengel, S.: Role of Hybrid Charge Transfer States in the Charge

Generation at ZnMgO/P3HT Heterojunctions. Journal of Physical Chemistry C **121**(40), 21955–21961 (2017). https://doi.org/10.1021/acs.jpcc.7b07293

[17] Benduhn, J., Tvingstedt, K., Piersimoni, F., Ullbrich, S., Fan, Y., Tropiano, M., McGarry, K.A., Zeika, O., Riede, M.K., Douglas, C.J., Barlow, S., Marder, S.R., Neher, D., Spoltore, D., Vandewal, K.: Intrinsic non-radiative voltage losses in fullerene-based organic solar cells. Nature Energy **2**(6) (2017). https://doi.org/10.1038/nenergy.2017.53

[18] Gierster, L., Vempati, S., Stähler, J.: Ultrashort and metastable doping of the ZnO surface by photoexcited defects. Faraday Discussions **237**, 58–79 (2022). https://doi.org/10.1039/d2fd00036a

[19] Vempati, S., Deinert, J., Gierster, L., Bogner, L., Richter, C., Mutz, N., Blumstengel, S., Zykov, A.: Uncovering the (un-) occupied electronic structure of a buried hybrid interface. Journal of Physics: Condensed Matter **31**(094001), 1–10 (2019)

[20] Ernstorfer, R., Gundlach, L., Felber, S., Storck, W., Eichberger, R., Willig, F.: Role of molecular anchor groups in molecule-to-semiconductor electron transfer. Journal of Physical Chemistry B **110**(50), 25383–25391 (2006). https://doi.org/10.1021/jp064436y

[21] Dimitrov, S., Schroeder, B., Nielsen, C., Bronstein, H., Fei, Z., McCulloch, I., Heeney, M., Durrant, J.: Singlet Exciton Lifetimes in Conjugated Polymer Films for Organic Solar Cells. Polymers **8**(1), 14 (2016). https://doi.org/10.3390/polym8010014

[22] Faulques, E., Wéry, J., Lefrant, S., Ivanov, V.G., Jonusauskas, G.: Transient photoluminescence of para-hexaphenyl layers. Physical Review B - Condensed Matter and Materials Physics **65**(21), 2122021–2122024 (2002). https://doi.org/10.1103/PhysRevB.65.212202

[23] Turkina, O., Nabok, D., Gulans, A., Cocchi, C., Draxl, C.: Electronic and optical excitations at the pyridine/ZnO($10\bar{1}0$) hybrid interface. Advanced Theory and Simulations **2**(2), 1800108 (2019) https://onlinelibrary.wiley.com/doi/pdf/10.1002/adts.201800108. https://doi.org/10.1002/adts.201800108

[24] Deinert, J.-C., Hofmann, O.T., Meyer, M., Rinke, P., Stähler, J.: Local aspects of hydrogen-induced metallization of the ZnO(10-10) surface. Physical Review B **91**(235313) (2015). https://doi.org/10.1103/PhysRevB.91.235313

[25] Ozawa, K., Sawada, K., Shirotori, Y., Edamoto, K.: Angle-resolved photoelectron spectroscopy study of the anion-derived dangling-bond band

on ZnO 101, 1–6 (2003). https://doi.org/10.1103/PhysRevB.68.125417

[26] Deinert, J.-C., Wegkamp, D., Meyer, M., Richter, C., Wolf, M., Stähler, J.: Ultrafast Exciton Formation at the ZnO (10-10) Surface. Physical Review Letters **113**(057602) (2014). https://doi.org/10.1103/PhysRevLett.113.057602

[27] Gierster, L., Vempati, S., Stähler, J.: Ultrafast generation and decay of a surface metal. Nature Communications **12**(978) (2021). https://doi.org/10.1038/s41467-021-21203-6

[28] Foglia, L., Vempati, S., Bonkano, B.T., Gierster, L., Wolf, M., Stähler, J., Vempati, S., Bonkano, B.T., Gierster, L.: Revealing the competing contributions of charge carriers, excitons, and defects to the non-equilibrium optical properties of ZnO. Structural Dynamics **6**(034501) (2019). https://doi.org/10.1063/1.5088767

[29] Gierster, L.: ZnO: Ultrafast photodoping - Ultrashort and metastable photoinduced metallization of the ZnO(10-10) surface. PhD Thesis, , Technische Universität Berlin (2021)

[30] Zhukov, V.P., Echenique, P.M., Chulkov, E.V.: Two types of excited electron dynamics in zinc oxide. Physical Review B - Condensed Matter and Materials Physics **82**(9), 1–8 (2010). https://doi.org/10.1103/PhysRevB.82.094302

[31] Diebold, U., Koplitz, L.V., Dulub, O.: Atomic-scale properties of low-index ZnO surfaces. Applied Surface Science **237**(1-4), 336–342 (2004). https://doi.org/10.1016/S0169-4332(04)00985-7

[32] Gulans, A., Kontur, S., Meisenbichler, C., Nabok, D., Pavone, P., Rigamonti, S., Sagmeister, S., Werner, U., Draxl, C.: exciting: a full-potential all-electron package implementing density-functional theory and many-body perturbation theory. Journal of Physics: Condensed Matter **26**(36), 363202 (2014). https://doi.org/10.1088/0953-8984/26/36/363202

[33] Draxl, C., Scheffler, M.: The nomad laboratory: from data sharing to artificial intelligence. Journal of Physics: Materials **2**(3), 036001 (2019). https://doi.org/10.1088/2515-7639/ab13bb